Chinese Chemical Society | Xiamen University

Journal of Electrochemistry

Online First

11-15-2023

Stability of a Solid Oxide Cell Stack under Direct Internal-reforming of Hydrogen-blended Methane

Yafei Tang

Anqi Wu

Beibei Han

Hua Liu

Shanjun Bao

Wanglin Lin

Ming Chen

Wanbing Guan

Subhash C. Singhal

RESEARCH ARTICLE

DOI: 10.61558/2993-074X.3430 **Article ID:** 1006-3471(2023)00-0000-00

Http://electrochem.xmu.edu.cn

Stability of a solid oxide cell stack under direct internal-reforming of hydrogen-blended methane

Yafei Tang[a], Anqi Wu[a], Beibei Han[a], Hua Liu[b], Shanjun Bao[b], Wanglin Lin[c], Ming Chen[d], Wanbing Guan[a]*, Subhash C. Singhal[a]

a Key Laboratory of Advanced Fuel Cells and Electrolyzers cell Technology of Zhejiang Province, Ningbo Institute of Materials Technology and Engineering, Chinese Academy of Sciences, Ningbo, Zhejiang, 315201

b Zhejiang Qiming Electric Power Group CO.LTD, Zhoushan, Zhejiang 316099, China

c Ocean Research Center of Zhoushan, Zhejiang University, Zhoushan, Zhejiang 316021, China

d Department of Energy Conversion and Storage, Technical University of Denmark (DTU), Lyngby, Denmark

Keywords: Hydrogen-blended methane steam; Internal reforming; Stability; Solid oxide fuel cell stack

Abstract: In this work, the long-term stability of a direct internal-reforming solid oxide fuel cell stack (IR-SOFC stack) using hydrogen-blended methane steam reforming are investigated. The stack is operated for about 3000 h, with a degradation rate of about 2.3%·kh^{-1}; the voltage of the two cells in the stack increase 3.38 mV·kh^{-1} and 3.78 mV·kh^{-1}, respectively. The area specific resistance of the three metal interconnects in the stack increase by 0.276 Ω·cm^2, 0.254 Ω·cm^2, and 0.249 Ω·cm^2, respectively. The results prove the stability of the flat-tube solid oxide fuel cell stack during long-term operation. The degradation of the stack is caused by segregation of Cr on the surface of metal interconnects and the formation of $SrCrO_4$ insulating phase in the current collecting layer of the cathode, which result in an increase in the interfacial resistance and decrease the stack performance. The long-term performance of a flat-tube IR-SOFC stack can be further improved by suitably coating the metal interconnect surface. This work provides theoretical and experimental reference for the application of hydrogen-blended methane steam reforming in flat-tube IR-SOFC stacks.

Introduction

As an energy conversion device that directly converts chemical energy into electrical energy, solid oxide fuel cell (SOFC) has been widely used because of its high efficiency, cleanliness, and multi-fuel capability [1-5]. The high temperature (600°C -1000°C) operation of SOFC stack allows direct internal reforming of carbon-containing fuel, such as methanol, natural gas, methane, biogas, and coke oven gas [6, 7]. However, high catalytic activity of Ni particles in the cell anode tends to break the C-H and C-O bonds in the hydrocarbon fuel, resulting in the formation of carbon. The deposited carbon covers the active sites of the Ni catalyst and/or prevents gas diffusion, resulting in higher ohmic and polarization resistances that lead to performance degradation. As a result, carbon deposition further damages the anode structure and leads to cell cracking [8-11]. When natural gas is used as fuel gas, methane cracking reaction and carbon monoxide disproportionation reaction may occur on the anode side of SOFC, which become the source of carbon deposition. The reactions are as follows [12, 13]:

$$CH_4(g) \leftrightarrow C(s) + 2H_2(g) \quad \Delta H_{298K} = +75 kJ{\cdot}mol^{-1} \quad (1)$$

$$2CO(g) \leftrightarrow C(s) + CO_2(g) \quad \Delta H_{298K} = -131 kJ{\cdot}mol^{-1} \quad (2)$$

Some researchers have tried improving the carbon deposition resistance of SOFC by modifying the anode. Lin et al. [14] used 50%Cu-50%Ni/8YSZ as the anode material, and found that almost no carbon deposition occurred during 2 hours of methane cracking. Lee et al. [10] conducted a methane steam reforming experiment on an IR-SOFC with a high entropy alloy anode at 750°C; the cell operated stably for 30 hours at a discharge current of 100 mA·cm^{-2} with steam-to-carbon (S/C) ratio of 2, with no carbon deposition at the anode. Neofytidis et al. [13] modified NiO/GDC anode with Au-Mo by a deposition coprecipitation method, and the degradation rate of the SOFC with this material was 2.6 mV·h^{-1} after 140 hours operation. Zhang et al. [15] used $La_{0.6}Sr_{0.4}Co_{0.2}Fe_{0.8}O_{3-\delta}$ (LSCF) perovskite-type mixed ionic electronic conductor (MIEC) to modify the anode by infiltration; the modified cell was operated in methane at 750°C for 100 hours with almost no degradation.

Nevertheless, for Ni/YSZ anode supported SOFCs, when natural gas is used as fuel gas, carbon deposition can be suppressed through methods such as steam reforming, carbon dioxide reforming, partial oxygen reforming, and by increasing current [16, 17]. Because nickel is easily oxidized and agglomerated, dry reforming and steam reforming are often used for methane reforming. Due to the advantages of easy access, low cost, cleanliness and abundance, water vapor can be mixed with methane for direct steam reforming to generate electricity in flat-tube SOFC [18, 19]. In this case, the degree of carbon deposition can be effectively suppressed through steam reforming reactions shown in equations (3)-(4) [20]:

$$CH_4(g) + H_2O(g) \leftrightarrow CO(g) + 3H_2(g) \quad \Delta H_{298K} = +206 kJ{\cdot}mol^{-1} \quad (3)$$

$$CO(g) + H_2O(g) \leftrightarrow CO_2(g) + H_2(g) \quad \Delta H_{298K} = -41 kJ{\cdot}mol^{-1} \quad (4)$$

In this work, internal methane steam reforming was carried out in a flat-tube SOFC stack with the addition of hydrogen. The degradation of the internal components of the stack was

monitored by inserting probes inside the SOFC stack, to further investigate the effect of hydrogen-blended methane steam on the long-term durability of the stack. This study clarifies the stability and degradation mechanism of the SOFC stacks, and provides a reference for large-scale application of direct internal methane steam reforming in IR-SOFC stacks.

Experimental Section

A flat-tube anode-supported solid oxide fuel cell stack developed by H_2-Bank Technology Co., Ltd. (Ningbo, China), with an active area of 60 cm^2, was used in this work. The composition and the thickness of each functional layer in the cell are shown in Table 1, and the cell structure is shown in Figure 1a. The cell fabrication procedure has been reported in detail previously [21-23]. The SOFC stack used consisted of two cells, three interconnects, and two conductive plates. The interconnect in contact with the anode of the cell had no gas flow channel, while the interconnect in contact with the cathode (air electrode) of the cell had an air flow channel. The interconnect is assembled in series with the cell. To enhance current collection between the interconnects and the cells, nickel mesh is added to the anode contact surface of each cell, and $La_{0.6}Sr_{0.4}CoO_{3-\delta}$ (LSC) and Ni slurries are screen printed on the cathode and the anode of the cells, respectively. Glass sealing material is used between the cell and the interconnect to seal the main body of the stack; the structure of the main body of the stack is shown in Figure 1b. After assembling the main body of the stack, mica sheets are used for pressure encapsulation. Finally, gas chambers are fixed and glass sealing materials are used to seal the stack; the completed stack is shown in Figure 1c.

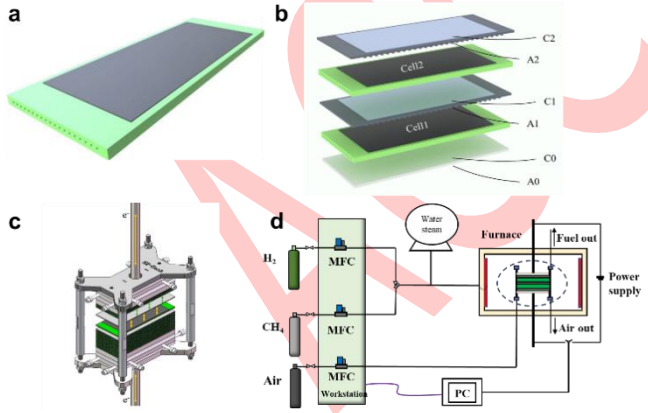

Figure 1. Schematic diagram of (a) cell structure, (b) stack assembly method, (c) physical diagram of stack, and (d) test system.

To investigate the degradation mechanism of the stack and monitor the degradation of each component inside the stack, voltage probes are inserted at the contact surface between the cell and the interconnect during the fabrication of the stack, as shown in the structural schematic diagram in Figure 1b. Before raising temperature, the gas pipes and conductive columns are installed, and the stack is placed in a furnace and heated at a rate of 2-5 °C·min^{-1}. A schematic diagram of the testing system is shown in Figure 1d.

Table 1. Parameters of SOFC

Composition	Material	Thickness
Supporting layer	NiO-3YSZ (3 mol. % yttria stabilized zirconia)	2.8 mm
Anode	NiO-8YSZ (8 mol. % yttria stabilized zirconia)	10 μm
Electrolyte	8YSZ (8 mol. % yttria stabilized zirconia)	10 μm
Barrier layer	GDC ($Gd_{0.1}Ce_{0.9}O_{2-\delta}$)	2 μm
Cathode	LSCF ($La_{0.6}Sr_{0.4}Co_{0.2}Fe_{0.8}O_{3-\delta}$) - GDC	15 μm
Buffer layer	LSC ($La_{0.6}Sr_{0.4}CoO_{3-\delta}$)	150 μm

After heating to the reaction temperature (750°C), 1 SLM of nitrogen is introduced to test the gas tightness of the stack, and then the fuel electrode is purged with N_2 for 10-15 minutes to exhaust air from the system. After purging with N_2, the fuel electrode is filled with 0.4 SLM H_2, and the air electrode is filled with 1.2 SLM air for stack reduction. This reduction usually takes 3-4 hours to convert NiO in anode to Ni, and after the open circuit voltage (OCV) stabilizes, the initial stack performance tests are carried out.

The initial performance was tested with a mixture of hydrogen, methane, and steam in the fuel electrode, with flow rates of 0.4, 0.3, and 0.9 SLM (S/C = 3), respectively. During the test, 4 SLM air was introduced to the air electrode. The initial performance was tested with a 100 W SOFC test system. After evaluating the initial performance, a long-term constant current discharge experiment was conducted to test the durability of hydrogen-blended methane steam reforming in direct internal-reforming flat-tube SOFC stack. During the long-term operation, the discharge performance of each component in the stack were measured at regular intervals.

After the long-term test, the stack was cooled to room temperature at a rate of 1°C·min^{-1} and disassembled for microstructural analysis. Flat, contamination-free cell samples were prepared to observe the cross-sections with a scanning electron microscope (S-4800, Hitachi, Japan). The center positions of the interconnects were cut into 5 mm ×10 mm specimens, then fill the samples with resin and polish the cross-sections of the stainless-steel interconnects for elemental analysis with energy dispersive X-ray spectroscopy (FEI Quanta FEG250, Hitachi, Japan). Raman spectroscopy (Renishaw inVia Reflex, UK), with a wavelength of 532 nm, was used for characterizing the buffer layer between the cathode and the interconnect, and for analyzing any carbon deposition in the fuel electrode.

Results and Discussion

Methane in the mixed fuel gas is completely reformed, when the gas injected into the fuel electrode of the stack is

$H_2/CH_4/H_2O$ at 0.4/0.3/0.9 SLM flow rates, respectively, as shown in Table 2. This indicates no carbon deposition during initial stack operation. Figure 2 shows the discharge performance curves of the SOFC stack in a hydrogen-blended methane steam environment, which were obtained at about runtimes of 0 h, 1000 h, 2000 h, and 3000 h. At these times, the open circuit voltages of the stack were 1.988 V, 1.983 V, 1.967 V, and 1.957 V, respectively. There was no significant fluctuation in the open circuit voltage of the stack during the discharge process of about 3000 hours, indicating that the stack maintained good airtightness, which eliminated the impact of any leaks on the stack performance. In order to describe the changes in the performance of the stack during the discharge process in detail, the performance data of the stack at 16 A is used as the reference. At the discharge voltage of 16 A (0.27 A · cm^{-2}), the corresponding voltages were 1.682 V, 1.679 V, 1.677 V, and 1.560 V, respectively, and the corresponding powers were 26.88 W, 26.83 W, 26.79 W, and 24.94 W, as shown in Figure 2a. After discharging for 2000 hours, the output power of the stack decreased by about 0.09 W; after running for another 1000 hours, the output performance of the stack decreased by approximately 1.94 W, and the performance of the stack has decreased by 7.2%.

Figures 2b and 2c show the I-V-P curves of Cell-1 and Cell-2 of the stack. The results showed that at 0 h, 1000 h, 2000 h, and 3000 h, the power at 16 A of Cell-1 was 13.55 W, 13.74 W, 13.80 W, and 13.53 W, respectively, and the power at 16 A of Cell-2 was 14.18 W, 14.27 W, 14.87 W, and 14.45 W, respectively. Obviously, the instantaneous performances of Cell-1 and Cell-2 indicate no degradation during operation.

Figures 2d, 2e, and 2f show the V-t curves of the stack and the cells operating at a discharge current of 16 A. The stack was operated for about 3000 hours, and the corresponding voltage and degradation rate are shown in Table 3. The results show that the voltage degradation rate of the stack after 3000 hours discharge is about 40.85 mV·kh^{-1}, approximately 2.3%·kh^{-1}. The results showed that during long-term operation, the performance of Cell-1 in Figure 2e steadily increased at a rate of approximately 3.47 mV·kh^{-1}, while the performance of Cell-2 in Figure 2f fluctuated and increased at a rate of approximately 3.82 mV·kh^{-1}. These results show that the performance degradation of SOFC stack during long-term operation when using hydrogen blended methane steam as fuel gas for direct internal reforming is independent of the cell, indicating good long-term durability of the flat-tube anode supported IR-SOFC.

Table 2. The content of each gas component after fuel gas reforming (%).

Gas	H_2	CH_4	CO	CO_2
After reforming	78.19	0	13.88	7.93

Table 3. Long-term operating performance of the SOFC stack under a constant current of 16 A.

	V_{start} (V)	V_{end} (V)	ΔV (mV)	η (mV·kh^{-1})
Stack	1.753	1.632	-121	-40.85
Cell-1	0.860	0.870	10.0	3.47
Cell-2	0.906	0.918	11.2	3.82

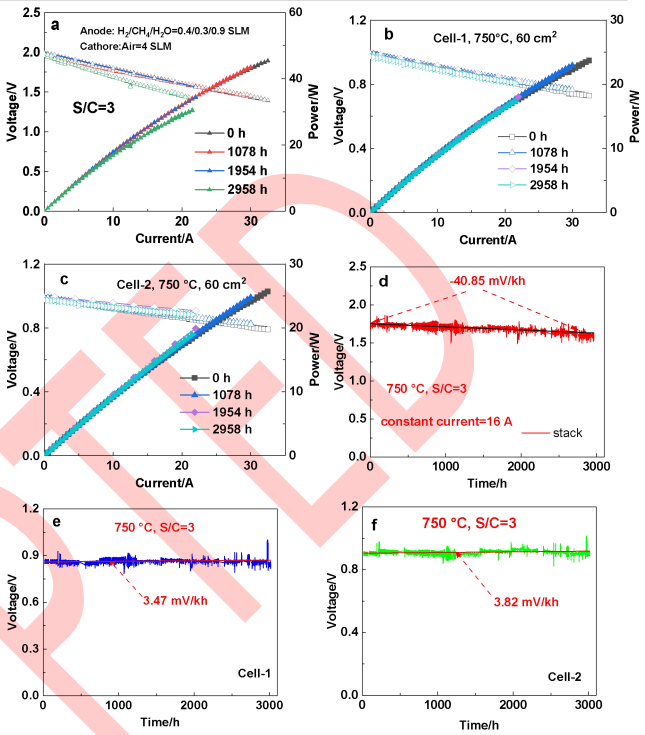

Figure 2. Discharge performance in hydrogen-blended methane steam: (a) I-V-P polarization curve of stack (b) I-V-P polarization curve of Cell-1 (c) I-V-P polarization curve of Cell-2; (d) V-t curve of stack e V-t curve of Cell-1 f V-t curve of Cell-2.

To study the impact of the interconnects inside the stack on its performance, the changes in the performance of the interconnects during 16 A discharge were analyzed, and the results are shown in Figure 3. The voltage of each interconnect is obtained by subtracting the voltage of a single cell from the voltage between the cell and the interconnect unit. Figure 3 shows the real-time voltage of the metal interconnects during the long-term discharge test. Through fitting calculation, the growth rate of the voltage of three metal interconnects is 24.81 mV·kh^{-1}, 22.82 mV·kh^{-1} and 23.14 mV·kh^{-1}, respectively. During the 3000-hour long-term operation, the area specific resistance of interconnect-1 (A_0-C_0 in Figure 1b) increased from 0.0353 Ω·cm^2 to 0.3114 Ω·cm^2, the area specific resistance of interconnect-2 (A_1-C_1 in Figure 1b) increased from 0.0356 Ω·cm^2 to 0.2894 Ω·cm^2, and for interconnect-3 (A_2-C_2 in Figure 1b), increased from 0.2588 Ω·cm^2 to 0.5188 Ω·cm^2. The area specific resistance corresponding to three interconnects increased by 0.276 Ω·cm^2, 0.254 Ω·cm^2, and 0.249 Ω·cm^2, respectively, with increase rates of approximately 0.0936 Ω·cm^2·kh^{-1}, 0.0864 Ω·cm^2·kh^{-1}, and 0.083 Ω·cm^2·kh^{-1}, as shown in Table 4. Obviously, the interconnects used in this work cannot meet the reported application requirements of less than 0.1 Ω·cm^2 [24].

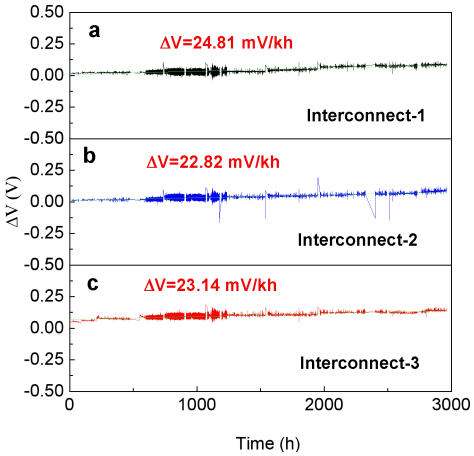

Figure 3. Real-time voltage of interconnects during long-term operation: (a) interconnect-1; (b) interconnect-2; (c) interconnect-3.

Table 4. Performance variation of interconnects under long-term constant current discharge with hydrogen-blended methane steam.

Interconnects	1	2	3
V_{start} (V)	0.0094	0.0096	0.0690
V_{end} (V)	0.0830	0.0773	0.1384
ASR_{start} ($\Omega \cdot cm^2$)	0.0353	0.0356	0.2588
ASR_{end} ($\Omega \cdot cm^2$)	0.3114	0.2894	0.5188
ΔV (mV)	73.6	67.7	69.3
η_1 ($mV \cdot kh^{-1}$)	24.81	22.82	23.14
η_2 ($\Omega \cdot cm^2 \cdot kh^{-1}$)	0.276	0.254	0.249

Figure 4 shows the microstructure of a reference cell (only reduced anode, without any electrochemical test) and the cell after long-term operation. No fracture or layering was found on the anode sides of Cell-1 and Cell-2. In addition, ImageJ software was used to analyze the agglomeration of nickel and calculate the distribution of nickel particles. The results showed that compared to the fuel electrodes of the reference cell, Cell-1, and Cell-2, the proportion of nickel within 0.6 μm² is 67.4%, 65.2%, and 69.4%, respectively, further indicating that the degree of nickel agglomeration is not significant. The structure of the three-phase boundary is intact ensuring long-term electrochemical reaction. This integrity of cell structure is the main reason for maintaining catalytic activity of the cell in long-term operation.

To verify any carbon deposition in the gas channels during long-term operation, Raman spectroscopy was used to characterize the inlet, middle, and outlet of the cell, and the results are shown in Figure 5. No carbon peaks (G and D peaks) appeared in the Raman spectrum, indicating no carbon deposition inside the cell during the long-term operation of the stack [25]. As a consequence, even under high water/carbon ratio (S/C=3), any non-uniformity of the mixed gas and uneven gas distribution inside the stack should not affect the methane reforming reaction.

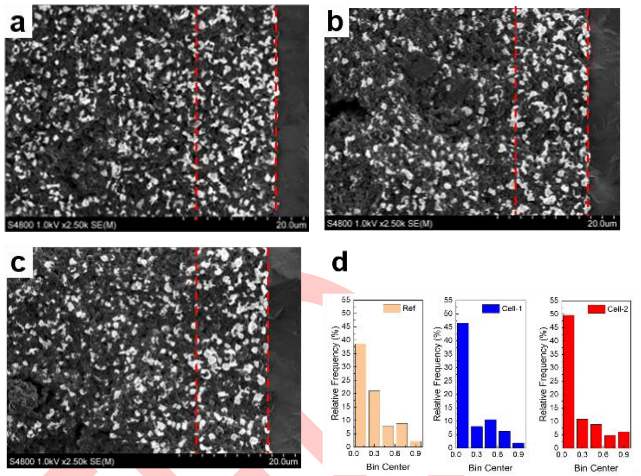

Figure 4. SEM images of the cell anode: (a) reference cell; (b) Cell-1; (c) Cell-2 (the area between red dashed line is the active anode); (d) Nickel particle distribution.

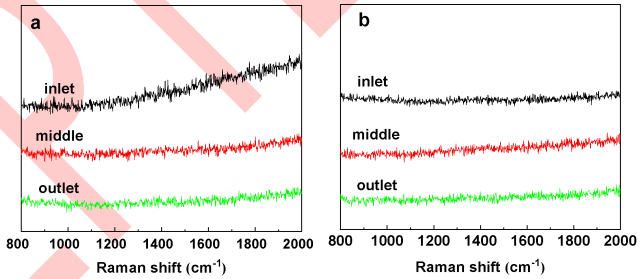

Figure 5. Raman spectra of the inlet, middle, and outlet of the gas channel of the cells: (a) Cell-1; (b) Cell-2.

In order to explore the changes in elemental content of the metal interconnects during testing, the interconnect-2 was selected to prepare 5 mm ×10 mm samples which were characterized by EDS at different positions.

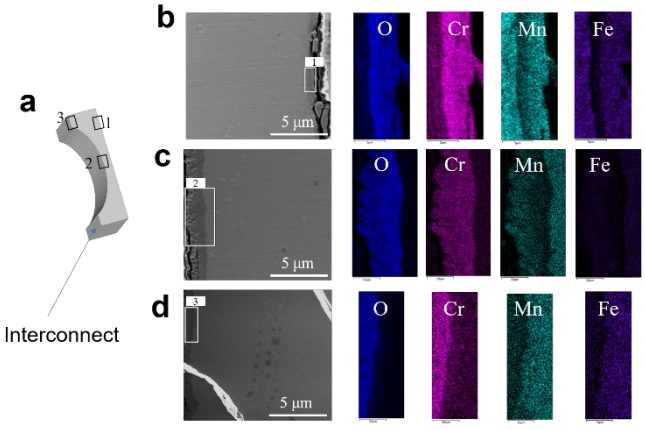

Figure 6. EDX of interconnect-2 at different positions: (a) Simulation diagram; (d) 1; (c) 2; (d) 3.

Figure 6 shows the EDX of interconnect-2 at different positions, which are the anode side (1), air flow channel (2), and ridge of the interconnect (3). It can be seen that there are varying degrees of oxidation at all three positions of the interconnect. Figure 6b shows the generation of a three-layer structure on the anode side of the interconnect. The surface is an oxide of iron, which is because when there is current passing through the connecting piece, a dense oxide layer cannot be formed in the reducing atmosphere. However, Fe diffuses to the surface and is oxidized. In the middle, Mn and Cr formed a Mn-Cr spinel, and the innermost oxide layer is Cr_2O_3 [26-29]. Figure 6c shows the formation of a two-layer structure on the surface (cathode surface) of the air flow channel, with the outermost layer being a Mn-Cr spinel and the inner layer being Cr_2O_3. Figure 6d shows the position where the cathode contacts the interconnect, and it can be inferred from the figure that Cr_2O_3 is mainly generated at the ridge. The results indicate that the connections inside the stack undergo varying degree of oxidation during operation, leading to a continuous increase in the surface specific resistance of the interconnections and a decrease in the stack performance.

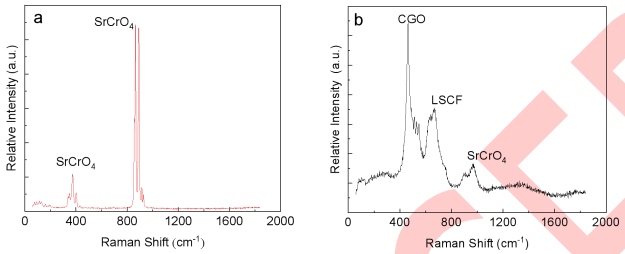

Figure 7. Raman spectroscopy analysis of the buffer layer on the cathode side after long-term test of the stack: (a) Cell-1; (b) Cell-2.

Figure 7 shows the Raman spectrum of the buffer layer (LSC) of the cell cathode after long-term operation. Buffer layers on the cathode side of Cell-1 (Figure 7a) and Cell-2 (Figure 7b) both exhibit sharp double peaks with Raman shifts of 865 cm^{-1} and 895 cm^{-1}, indicating the generation of $SrCrO_4$ phase [30, 31]. Research has shown that under long-term operation of the IR-SOFC stack with methane steam, Cr rich phase will generate on the surface of the interconnects, which leads to the formation of $SrCrO_4$ in the buffer layer, thereby accelerating the performance degradation of the interconnects. The degradation of the interconnects is the result of poor high-temperature oxidation resistance, cathode poisoning caused by volatile Cr, and high area specific resistance [32-34]. Therefore, it is necessary to develop protective coatings for metal interconnects.

Conclusion

This work investigated the stability and degradation mechanism of a flat-tube solid oxide fuel cell stack through about 3000 h high-temperature operation on direct internal reforming of hydrogen-blended methane steam. The overall degradation rate of the stack was about 2.3%·kh^{-1}, with an increase of 10.0 mV (3.38 mV·kh^{-1}) for Cell-1 and 11.2 mV (3.78 mV·kh^{-1}) for Cell-2, respectively. The microstructural characterizations of the cell and cell/interconnect surfaces were used for further analyzing the reason for degradation; these showed integrity of the cell structure, no obvious Ni agglomeration on the anode side, and no carbon deposition in the gas channel and active anode. The results indicate that flat-tube SOFC stack has good tolerance in hydrogen-blended methane steam environments. The area specific resistance of the three interconnects in the cell stack increased at rates of 0.276 Ω·cm^2·kh^{-1}, 0.254 Ω·cm^2·kh^{-1}, and 0.249 Ω·cm^2·kh^{-1}, respectively. Through EDX characterization of the cross-sections of the metal interconnects and Raman spectroscopy analysis of the cell/interconnect surface, chromium rich oxide layer was found on the surface of the metal interconnects, and $SrCrO_4$ insulation phase was observed in the LSC buffer layer. After 3000 hours of operation under hydrogen-blended methane steam in the SOFC stack, an oxide layer formed on the outside of the metal interconnects of the cell stack, resulting in a degradation rate of 2.3%·kh^{-1}. It is therefore necessary to apply protective surface coatings on metal interconnects to suppress oxide formation and performance deterioration during long-term operation, which can greatly improve the stability of the SOFC stack.

Acknowledgements

We gratefully acknowledge the National Key Research and Development Program of China (No. 2022YFB4003602), National Natural Science Foundation of China (U20A20251, 11932005), Key R & D projects in Zhejiang Province (2021C01101), Ningbo Key R&D project (2023Z145).

References

[1] Hanif H B, Motola M, Qayyum S, Rauf S, Khalid A, Li C J, Li C X. Recent advancements, doping strategies and the future perspective of perovskite-based solid oxide fuel cells for energy conversion [J]. Chem. Eng.J., 2022, 428: 132603.

[2] Hua B, Li M, Sun Y F, Zhang Y Q, Yan N, Li J, Etsell T, Sarkar P, Luo J L. Grafting doped manganite into nickel anode enables efficient and durable energy conversions in biogas solid oxide fuel cells[J]. Appl. Catal. B Environ., 2017, 200: 174-181.

[3] Zhuang Z C, Li Y H, Yu R H, Xia L X, Yang J R, Lang Z Q, Zhu J X, Huang J Z, Wang J O, Wang Y, Fan L D, Wu J S, Zhao Z, Wang D S, Li Y D. Reversely trapping atoms from a perovskite surface for high-performance and durable fuel cell cathodes[J]. Nat. Catal., 2022, 5: 300-310.

[4] Yang Y, Li T, Feng P Z, Wang X X, Wang S R, Li Y H, Shao Z P. Highly efficient conversion of oxygen-bearing low concentration coal-bed methane into power via solid oxide fuel cell integrated with an activated catalyst-modified anode microchannel[J]. Appl. Energy, 2022, 328: 120134.

[5] Alaedini A H, Tourani H K, Saidi M. A review of waste-to-hydrogen conversion technologies for solid oxide fuel cell (SOFC) applications: Aspect of gasification process and catalyst development[J]. J. Environ. Manage., 2023, 329: 117077.

[6] Kupecki J, Motylinski K, Milewski J. Dynamic analysis of direct internal reforming in a SOFC stack with electrolyte-supported cells using a quasi-1D model[J]. Appl. Energy, 2018, 227: 198-205.

[7] Menon V, Banerjee A, Dailly J, Deutschmann O. Numerical analysis of mass and heat transport in proton-conducting SOFCs with direct internal reforming[J]. Appl. Energy, 2015, 149: 161-175.

[8] Sang J K, Liu S, Yang J, Wu T, Luo X, Zhao Y M, Wang J X, Guan W B, Chai M R, Singhal S C. Power generation from flat-tube solid oxide fuel cells by direct internal dry reforming of methanol: A route for simultaneous utilization of CO_2 and biofuels[J]. Chem. Eng.J., 2023, 457: 141189.

[9] Fan L Y, Li C E, Aravind P V, Weiwei Cai d, Han M F, Brandon N. Methane reforming in solid oxide fuel cells: Challenges and strategies[J]. J. Power Sources, 2022, 538: 231573.

[10] Lee K X, Hu B X, Dubey P K, Anisur M R, Belko S, Aphale A N, Singh P. High-entropy alloy anode for direct internal steam reforming of methane in SOFC[J]. Int. J. Hydrog. Energy, 2022, 47(90): 38372-38385.

[11] Lanzini A, Leone P, Guerra C, Smeacetto F, Brandon N P, Santarelli M. Durability of anode supported Solid Oxides Fuel Cells (SOFC) under direct dry-reforming of methane[J]. Chem. Eng.J., 2013, 220: 254-263.

[12] Zhang H, Liu W, Wang J X, Yang J, Chen Y, Guan W B, Singhal S C. Power generation from a symmetric flat-tube solid oxide fuel cell using direct internal dry-reforming of methane[J]. J. Power Sources, 2021, 516: 230662.

[13] Niakolas D K, Ouweltjes J P, Rietveld G, Dracopoulos V, Neophytides S G. Au-doped Ni/GDC as a new anode for SOFCs operating under rich CH4 internal steam reforming[J]. Int. J. Hydrog. Energy, 2010, 35(15): 7898-7904.

[14] Lin Y C, Wei W C J. Porous Cu–Ni-YSZ cermets using CH_4 fuel for SOFC. Int. J. Hydrog. Energy, 2020, 45(46): 24253-24262.

[15] Zhang Y L, Xu N, Fan H, Han M F. $La_{0.6}Sr_{0.4}Co_{0.2}Fe_{0.8}O_{3-\delta}$ nanoparticles modified Ni-based anode for direct methane-fueled SOFCs[J]. Energy Procedia, 2019, 158: 2250-2255.

[16] Lin K W, Wu H W. Hydrogen-rich syngas production and carbon dioxide formation using aqueous urea solution in biogas steam reforming by thermodynamic analysis[J]. Int. J. Hydrog. Energy, 2020, 45(20): 11593-11604.

[17] Kalai D Y, Stangeland K, Jin Y Y, Tucho W M, Yu Z X. Biogas dry reforming for syngas production on La promoted hydrotalcite-derived Ni catalysts[J]. Int. J. Hydrog. Energy, 2018, 43(42): 19438-19450.

[18] Labanca A R C, Cunha A G, Ribeiro R P, Zucolotto C G, Cevolani M B, Schettino M A. Technological solution for distributing vehicular hydrogen using dry plasma reforming of natural gas and biogas[J]. Renew. Energy, 2022, 201: 11-21.

[19] de Souza T A Z, Coronado C J R, Silveira J L, Pint G M. Economic assessment of hydrogen and electricity cogeneration through steam reforming-SOFC system in the Brazilian biodiesel industry[J]. J. Clean Prod., 2021, 279: 123814.

[20] Chou Y S, Huang M H, Hsu N Y, Jeng K T, Lee R Y, Yen S C. Development of ring-shape supported catalyst for steam reforming of natural gas in small SOFC systems[J]. Int. J. Hydrog. Energy, 2016, 41(30): 12953-12961.

[21] Wu A Q, Li C L, Han B B, Hanson S, Guan W B, Singhal S C. Effect of air addition to the air electrode on the stability and efficiency of carbon dioxide electrolysis by solid oxide cells[J]. Int. J. Hydrog. Energy, 2016, 47(58): 24268-24278.

[22] Wu A Q, Li C L, Han B B, Liu W, Zhang Y, Hanson S, Guan W B, Singhal S C. Pulsed electrolysis of carbon dioxide by large-scale solid oxide electrolytic cells for intermittent renewable energy storage[J]. Carbon Energy, 2023, 5(4): 1-12.

[23] Li C L, Wu A Q, Xi C Q, Guan W B, Chen L, Singhal S C. High reversible cycling performance of carbon dioxide electrolysis by flat-tube solid oxide cell[J]. Appl. Energy, 2022, 314: 118969.

[24] Hu Y Z, Gao J T, Li C X, Li C J. Thermally sprayed MCO/FeCr24 interconnector with improved stability for tubular segmented-in-series SOFCs[J]. Appl. Surf. Sci., 2022, 587: 152861.

[25] Peña-Álvarez M, del Corro E, Langa F, Baonzaa V G, Taravillo M. Morphological changes in carbon nanohorns under stress: a combined Raman spectroscopy and TEM study[J]. RSC Adv., 2016, 6: 49543-49550.

[26] Tan K H, Rahman H A, Taib H. Coating layer and influence of transition metal for ferritic stainless steel interconnector solid oxide fuel cell: A review[J]. Int. J. Hydrog. Energy, 2016, 44(58): 30591-30605.

[27] Xu Y J, Wang S R, Liu R Z, Wen T L, Wen Z Y. A novel bilayered $Sr_{0.6}La_{0.4}TiO_3/La_{0.8}Sr_{0.2}MnO_3$ interconnector for anode-supported tubular solid oxide fuel cell via slurry-brushing and co-sintering process[J]. J. Power Sources, 2011, 196(3): 1338-1341.

[28] Horita T, Kishimoto H, Yamaji K, Xiong Y P, Sakai N, Brito M E, Yokokawa H. Oxide Scale Formation and Stability of Fe-Cr Alloy Interconnects under Dual Atmospheres and Current Flow Conditions for SOFCs[J]. J. Electrochem. Soc., 2006, 153: A2007.

[29] Horita T, Kshimoto H, Yamaji K, Sakai N, Xiong Y P, Brito M E, Yokokawa H. Anomalous oxidation of ferritic interconnects in solid oxide fuel cells[J]. Int. J. Hydrog. Energy, 2008, 33(14): 3962-3969.

[30] Zhao L, Zhang J, Becker T, Jiang S P. Raman Spectroscopy Study of Chromium Deposition on $La_{0.6}Sr_{0.4}Co_{0.2}Fe_{0.8}O_{3-\delta}$ Cathode of Solid Oxide Fuel Cells[J]. J. Electrochem. Soc., 2014, 161: F687.

[31] Li X X, Blinn K, Chen D C, Liu M L. In Situ and Surface-Enhanced Raman Spectroscopy Study of Electrode Materials in Solid Oxide Fuel Cells[J]. Electrochem. Energy Rev., 2018, 1: 433-459.

[32] Church B C, Sanders T H, Speyer R F, Cochran J K. Thermal expansion matching and oxidation resistance of Fe-Ni-Cr interconnect alloys[J]. Mater. Sci. Eng. A-Struct. Mater. Prop. Microstruct. Process., 2007, 452-453: 334-340.

[33] Wu J W, Liu X B. Recent Development of SOFC Metallic Interconnect[J]. J. Mater. Sci. Technol., 2010, 26(4): 293-305.

[34] Tkachenko S, Brodnikovskyi D, Cizek J, Komarov P, Brodnikovskyi Y, Tymoshenko Y, Csáki Š, Pinchuk M, Vasylyev O, Čelko L, Gadzyra M, Chráska T. Novel Ti-Si-C composites for SOFC interconnect materials: Production optimization[J]. Ceram. Int., 2022, 48(19): 27785-27798.

以掺氢天然气为燃料直接内重整固体氧化物电池堆的稳定性

汤亚飞[a]，武安祺[a]，韩贝贝[a]，刘华[b]，包善军[b]，林王林[c]，陈铭[d]，官万兵[a*]，Subhash C. Singhal[a]

（a. 中国科学院宁波材料技术与工程研究所，浙江宁波镇海中官西路 1219 号，315201；b. 浙江启明电力集团有限公司，浙江舟山，316099；c. 浙江大学舟山海洋研究中心，浙江舟山，316021; d. 丹麦技术大学能源转换与储存系，丹麦）

摘要：本文研究了掺氢天然气直接内重整平管型固体氧化物电池短堆的长期稳定性和衰减机理。通过约 3000 小时的实测实验，结果显示：电堆的总体衰减率为 2.3%·kh^{-1}，电堆中三个金属连接板的面积比电阻分别增加了 0.276 Ω·cm^2、0.254 Ω·cm^2 和 0.249 Ω·cm^2，但电堆中两个电池的电压反而分别增加了 3.38 mV·kh^{-1} 和 3.78 mV·kh^{-1}。电堆衰减主要由金属连接件表层氧化及其与阴极集流层材料反应生成 $SrCrO_4$ 物质，两者共同作用增大了电池与金属连接体间的界面电阻所致。结果表明以掺氢天然气为燃料直接内重整平管型固体氧化物燃料电池电堆具有良好的稳定性。本文工作为掺氢天然气在固体氧化物燃料电池堆中的直接内重整应用提供了理论参考与实验依据。

关键词：掺氢天然气；内重整；稳定性；固体氧化物电堆

Entry for the Table of Contents